Wavelength-selective emitters with pyramid nanogratings enhanced by multiple resonance modes



2016 Nanotechnology 27 155402

(http://iopscience.iop.org/0957-4484/27/15/155402)

OPEN ACCESS
IOP Publishing
Nanotechnology

Nanotechnology **27** (2016) 155402 (9pp)
doi:10.1088/0957-4484/27/15/155402

# Wavelength-selective emitters with pyramid nanogratings enhanced by multiple resonance modes

**Nghia Nguyen-Huu**[1,2], **Jaromír Pištora**[2] **and Michael Cada**[1,2]

[1] Department of Electrical and Computer Engineering, Dalhousie University, Halifax, Nova Scotia N3H 4R2, Canada
[2] Nanotechnology Centre, VSB-Technical University of Ostrava, Ostrava-Poruba 708 33, Czech Republic

E-mail: nghia.nguyen-huu@dal.ca and nghianano@gmail.com

Received 15 September 2015, revised 8 December 2015
Accepted for publication 20 January 2016
Published 3 March 2016


**Abstract**

Binary gratings with high or low metal filling ratios in a grating region have been demonstrated as successful candidates in enhancing the emittance of emitters for thermophotovoltaics since they could support surface plasmons (SPs), the Rayleigh–Wood anomaly (RWA), or cavity resonance (CR) within their geometries. This work shows that combining a tungsten binary grating with a low and high filling ratio to form a pyramid grating can significantly increase the emittance, which is nearly perfect in the wavelength region from 0.6 to 1.72 $\mu$m, while being 0.1 at wavelengths longer than 2.5 $\mu$m. Moreover, the emittance spectrum of the hybrid tungsten grating is insensitive to the angle of incidence. The enhancement demonstrated by magnetic field and Poynting vector patterns is due to the interplay between SPs and RWA modes at short wavelengths, and CR at long wavelengths. Furthermore, a combined grating made of nickel is also proposed providing enhanced emittance in a wide angle of incidence.

Keywords: thermal emission, nanostructures, thermophotovoltaics, surface plasmons, Rayleigh–Wood anomaly, cavity resonance, metals

(Some figures may appear in colour only in the online journal)

## 1. Introduction

Thermophotovoltaic (TPV) devices used to generate electricity directly from heat have attracted great attention since they could solve many problems of conventional energy resources such as cleanness, portability, or low maintenance [1]. In principle, a TPV emitter is heated up by burning fossil fuel or using waste heat, and its thermal radiation is then absorbed by a TPV cell which converts the photon energy into electricity. The conversion happens when the incoming wavelength is shorter than the wavelength corresponding to the bandgap of the TPV cells. An ideal emitter needs have a high emittance at the working wavelength of TPV cells and low emittance at longer wavelengths. In addition, the emitter should be insensitive to the incident direction in order to efficiently absorb energy coming from different directions. Accordingly, researchers have put a lot of effort into finding efficient emitters to improve the conversion efficiency.

One-dimensional (1D), 2D, and 3D nanostructures have provided excellent solutions for TPV applications with the enhancement of emittance based on many physical mechanisms [2–32]. For example, 1D deep gratings and 2D microcavities could increase the emission based on cavity resonance modes [12, 33]. Moreover, the gratings can also excite surface plasmons or magnetic polaritons (MPs) at their horizontal and vertical metal boundaries or inside their slits [8, 13, 14, 34]. Many researchers using different evolutionary optimizations and design-based physical studies have tried various grating structures with rectangular, triangular, or blazed profiles to achieve maximum emittance [2–9, 11–15, 17–25, 35]. However, very few studies have considered



 

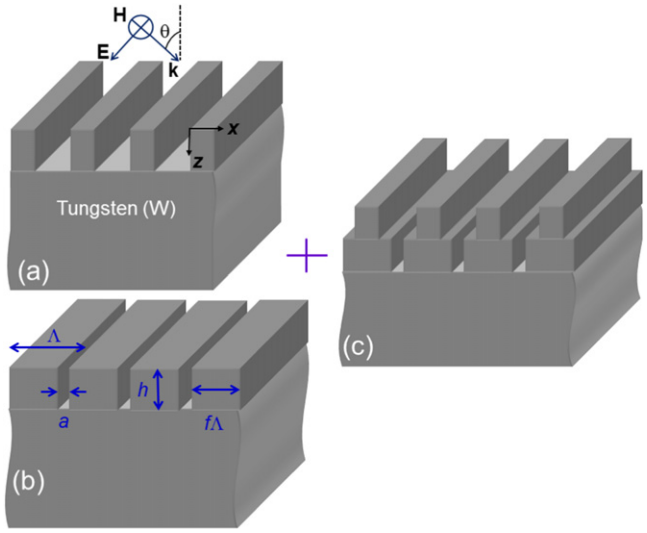


**Figure 1.** (a) and (b) Schematics of TPV emitters made of a tungsten grating on tungsten substrate with grating period Λ, grating thickness $h$, variable filling ratio $f$, and groove width $a$. (c) TPV emitter constructed from (a) and (b).

investigations of physical origins in enhancing emittance of a pyramid grating structure combining a low filling ratio grating layer with a high one, which exhibits nearly perfect emission for TPV applications.

In this paper, a pyramid grating structure as an emitter featuring a nearly perfect emittance (close to 1) in the wavelength region from 0.6 to 1.72 $\mu$m and a very low one (below 0.1) at wavelengths longer than 2.5 $\mu$m is demonstrated. The emittance enhancement due to the interplay of the Rayleigh–Wood anomaly (RWA) and surface plasmons (SPs), and cavity resonance (CR) modes is also confirmed based on analytic solutions and calculations of near-field magnetic patterns and time-average Poynting vectors.

## 2. Model development and numerical method

### 2.1. Geometry and material

The structure shown in figures 1(a) and (b) comprises a tungsten (W) grating atop an opaque W substrate, whose profiles are much preferred compared with those of 2D and 3D structures due to ease of fabrication [36] and its performance is acceptable [2–5, 8, 9, 11]. Figures 1(a) and (b) illustrate a grating layer with a low filling ratio and a grating with a high one, respectively, while figure 1(c) shows a combined grating structure as a pyramid grating. The geometric parameters include the grating period Λ, the grating thickness $h$, the metal filling ratio in the grating region $f$, and the groove width $a$. W and nickel (Ni) are selected as the emitter's materials due to their high melting points and strong resistivity against corrosion. This is also because various proposed emitters/absorbers constructed on multilayer, multimaterial, and metal-dielectric composite coating structures cannot withstand high temperatures less than 2000 K (considered in this study) due to thermomechanical stresses and chemical reactions between and within their layers. The optical constants of W and Ni are simulated with the Drude–Lorentz model [37]. The emittance or absorptance can be obtained from Kirchhoff's law, i.e., $A = 1 - R$, where $R$ is the reflectance calculated based on the rigorous coupled-wave analysis (RCWA) [34, 38, 39]. Only the transverse magnetic (TM) wave is considered here due to its enhancement attributed to many excitations including SPs, localized SPs, MPs, RWA, or CR compared with the transverse electric (TE) wave. It is incident on the grating layer depicted by a wavevector **k** and an incidence angle ($\theta$).

### 2.2. Design guidelines using a numerical method

Figures 2(a) and (b) show the normal emittance spectrum of a single-layered grating structure with varied grating thicknesses $h$, low and high filling ratios ($f = 0.1$ and 0.9), and a grating (constant) period of 400 nm. It is observed that the emittance of all grating structures shown in both figures is higher than that of the plain W surface. For structures with a low filling ratio ($f = 0.1$) as shown in figure 2(a), they do not exhibit a maximum value in a wide wavelength range. On the other hand, it is seen from figure 2(b) that the structures with a high filling ratio display higher emittance than those shown in figure 2(a). Moreover, the grating structure with a thickness of 200 nm and filling ratio of 0.9 provides high emittance in the wavelength range from 0.6 to 1.72 $\mu$m and a low one at wavelengths longer than 2.5 $\mu$m. As previously mentioned, the conversion of the photon energy to electrical power occurs when the wavelength of incident light is shorter than the bandgap wavelength of GaSb. However, the absorption of the emitted photon at wavelengths (e.g., $>2$ $\mu$m) longer than the bandgap wavelength cannot produce electron–hole pairs; as a result, the system cannot generate electricity. Meanwhile, the emittance at shorter wavelengths (e.g., $<0.6$ $\mu$m) is negligible because of its very low conversion efficiency according to Planck's blackbody spectral distribution.

Accordingly, the grating with the thickness of 200 nm, the grating period of 400 nm, and the filling ratio of 0.9 is selected as a reference for designing a nearly perfect thermophotovoltaic emitter for various reasons. First, it provides high emittance in the wavelength range of interest. Second, it is feasibly implemented using current fabrication techniques such as electron-beam lithography, focused ion beam lithography, and nanoimprint lithography because its aspect ratio, defined as the ratio of the grating thickness $h$ and the grating width ($w = \Lambda - a$), is comparable. Last, it has been shown that the spectral emittance of a simple binary W grating remains unchanged when modifying its geometric dimension by 5% [9]. On the other hand, a structure with a large thickness ($h = 1200$ nm) provides maximum emittance outside the wavelength range of interest and is challenging for fabrication due to having a large aspect ratio [40–43].

Figure 3 shows emittance contours for a single-layered W grating (see figures 1(a) and (b)) for TM waves at normal incidence as a function of the wavelength $\lambda$ and the grating period Λ with a fixed $h = 200$ nm and a varied $f = 0.1$, 0.4, 0.6, and 0.9. It is seen that the emittance from figures 3(b)–(d)

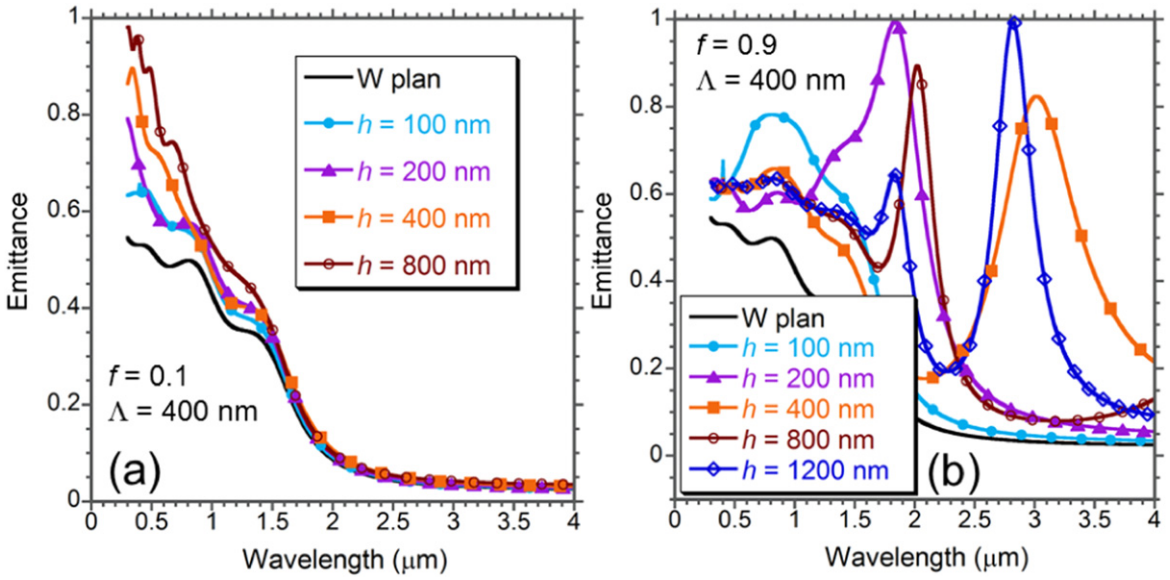


**Figure 2.** (a) and (b) Normal emittance spectrum of structures shown in figures 1(a) and (b) with different filling ratios ($f = 0.1$ and 0.9) and $h$ and a constant $\Lambda = 400$ nm for TM waves.

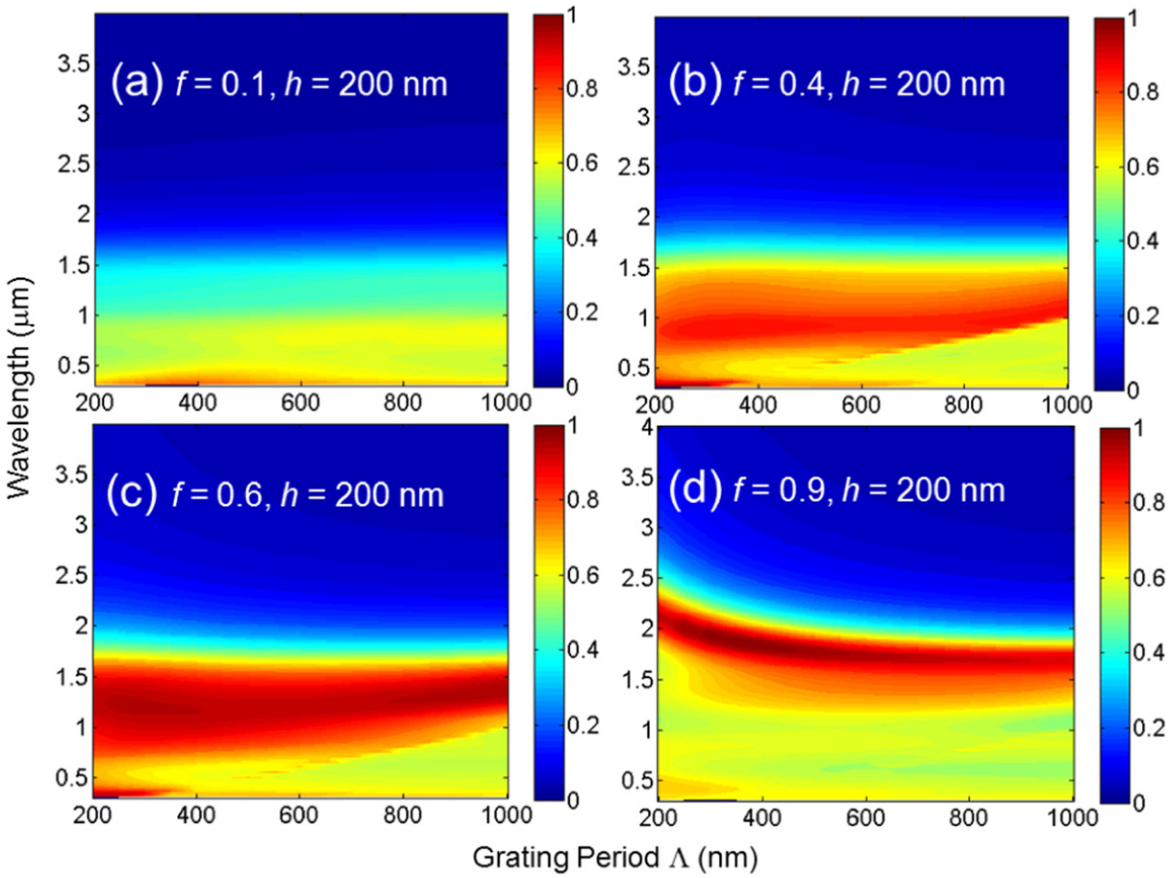


**Figure 3.** Emittance contour for single-layered grating structure with $h = 200$ nm for varying $\Lambda$ from 200 to 1000 nm: (a) $f = 0.1$, (b) $f = 0.4$, (c) $f = 0.6$, and (d) $f = 0.9$.

displays a higher value in a large range of the grating periods compared with that of figure 3(a). However, its spectrum does not cover the wavelength region of $0.6 \sim 1.72$ $\mu$m corresponding to the operating wavelength range of typical GaSb-related TPV cells [44]. Additionally, for a grating period with a large $f$ ($f = 0.9$), the maximum emittance occurs in a wavelength range from 1.6 to 2.4 $\mu$m, while for the other periods with a small $f$, it is maximum in a wavelength range of

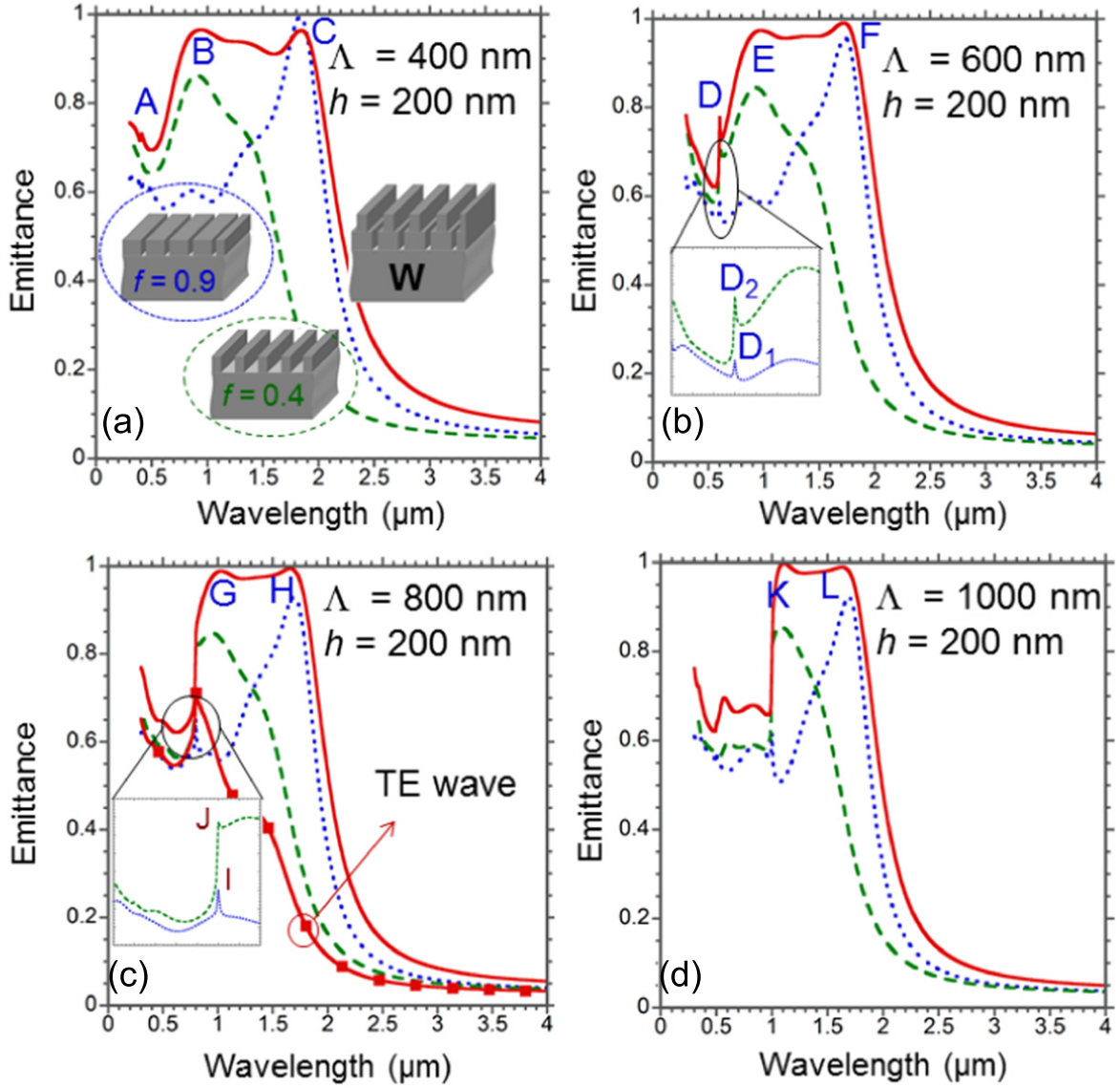


**Figure 4.** Emittance spectrum calculated for TM waves at normal incidence of grating structures with $h = 200$ nm, $f_1 = 0.4$, $f_2 = 0.9$, and (a) $\Lambda = 400$ nm, (b) $\Lambda = 600$ nm, (c) $\Lambda = 800$ nm, and (d) $\Lambda = 1000$ nm. It is noted that the red solid curve with rectangular marks in (c) shows the emittance spectrum calculated for the TE wave.

$0.6 \sim 1.5\ \mu$m. Consequently, we propose a grating comprising two single-layered gratings with different metal filling ratios. It is noted that the grating structure with a small value of $f_1$ is built on the grating with a larger one, $f_2$.

## 3. Mechanisms responsible for the emittance enhancement

Previous studies have shown that grating structures display extraordinary emission enhancement compared with plain metal surfaces due to excitations of SPs, RWA, and CR [9]. The resonance frequency that causes a sudden reduction of the reflectance (an increase of absorptance) can be predicted via analytical solutions as described below.

For the gratings with narrow grooves ($f = 0.9$) as shown in figure 1(b), the TM SP mode can be expressed by an effective medium approximation. The approximation method is used to calculate a three-layered structure including a homogeneous anisotropic layer (the grating layer) sandwiched between the dielectric (air) and metal layers. In order to find the SP wavevector of a wave propagating into the grating structure, one can match the non-zero components of magnetic and electric fields at the boundary $z = 0$, which can be found in [45]. After some derivations, the magnitude of the SP wavevector is thus given by:

$$\mathrm{k} = \left(\varepsilon_{\mathrm{d}}\mathrm{k}_0^2 + \left(\frac{a\varepsilon_{\mathrm{d}}}{\Lambda\varepsilon_{\mathrm{g}}}\right)^2 \mathrm{k}_{\mathrm{g}}^2 \tan^2(\mathrm{k}_{\mathrm{g}}h)\right)^{1/2} \quad (1)$$

Here $k_g$ is the wavevector magnitude of a wave propagating into the grooves, $k_0$ is the free space wavevector, and $\varepsilon_d$ and $\varepsilon_g$ are the dielectric functions of the above grating

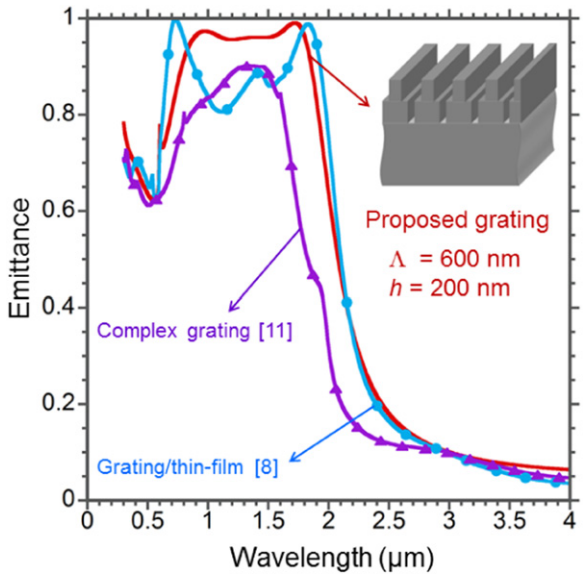


**Figure 5.** Comparison of emittance among the proposed structure with that of a 1D complex grating in [11] and a magnetic-polariton-enhanced TPV emitter in [8].

region (air) and grating grooves (air), respectively, with $\varepsilon_d = \varepsilon_g = \varepsilon_{air} = 1.0$.

For RWA, the absorptance/emittance spectrum is abruptly changed because one of the diffraction orders $j$ disappears at the grazing angle $\theta_d = \pm 90°$. RWA resonance can be expressed as [9, 46].

$$\left(\frac{\lambda}{\Lambda}j\right)^2 + 2\frac{\lambda}{\Lambda}j\sin\theta - \cos^2\theta = 0 \tag{2}$$

The CR mode occurs due to the interference effects with grating structures. It is defined as [12]

$$\lambda_{lmn} = \frac{2}{\sqrt{(l/L_x)^2 + (m/L_y)^2 + ((n+1/2)/L_z)^2}} \tag{3}$$

Here $l$, $m$, and $n$ are integers; $L_x$ and $L_z$ correspond to $a$ and $h$, respectively; and $L_y$ is infinite along the $y$ direction.

## 4. Emittance spectrum of grating structures and physical and analytical interpretation of grating response

Figure 4 shows the emittance spectrum for TM waves at normal incidence of three grating structures with geometric parameters $h = 200$ nm, $f_1 = 0.4$, and $f_2 = 0.9$ for different grating periods from 400 to 1000 nm. It is noted that the values of $\Lambda$, $h$, and $f$ are selected based on the above analysis in order to obtain high emittance in a large range of wavelengths of interest. It is seen that the emittance of the grating structures shown in figures 4(b) and (c) is obtained to be approximately 0.99 as labeled by E, F, G, and H, compared with that of figure 4(a). Although the emittance labeled by K and L of the structures in figure 4(d) is as high as in figures 4(b) and (c), it lies in a shorter wavelength range (e.g., $1.5\ \mu m < \lambda < 2.15\ \mu m$). Moreover, it is observed from figure 4(c) that the obtained emittance spectrum for the TE wave (the solid red curve with triangular marks) is much smaller than those for the TM waves although it also covers the wavelength range of interest. Interestingly, most hybrid grating structures exhibit higher emittance and a broader bandwidth than the single-layered grating structures. It is found that the emittance spectrum of the pyramid gratings superimposes two spectra of single-layered gratings. Moreover, the spectral characteristics of the single-layered gratings are similar, e.g., peaks $D_1$, $D_2$, I, and J, while those of the hybrid gratings are different, i.e., the disappearance of these peaks in figures 4(c) and (d).

For comparison, the emittance of complex grating [11] (the solid curve with triangular marks) and a magnetic-polariton-enhanced TPV emitter [8] (the solid curve with circle marks) is also generated by our codes as shown in figure 5. It is observed that the proposed emitter exhibits an average emittance (0.94) in the wavelength range from 0.6 $\mu$m to 1.72 $\mu$m higher than that of the complex grating (0.83) and of the emitter-based the magnetic polariton mode (0.88). Consequently, it is worth mentioning that the results presented in figures 4 and 5 illustrate efficiently designed emitters for TPV applications.

The directional emittance at peaks A, B, C, D, E, F, G, H, K, and L as shown in figure 4 at wavelengths of 0.47 $\mu$m, 0.94 $\mu$m, 1.84 $\mu$m, 0.60 $\mu$m, 0.98 $\mu$m, 1.72 $\mu$m, 1.03 $\mu$m, 1.66 $\mu$m, 1.10 $\mu$m, and 1.63 $\mu$m, respectively, is plotted in figure 6 to compare the angular dependence of the proposed structures. Figure 6(a) shows that emittance at peaks A, B, and C increases as the wavelength rises, but also increases with the emission angle up to a maximum and then reduces to zero when the angle is 90°. In figure 6(b), the emittance of the grating structure with $\Lambda = 600$ nm at peak F displays the highest value, above 0.85 from $\theta = 0°$ to 70° while that at peak E is obtained above 0.6 from $\theta = 0°$ to 70° and then drops to zero. At peak D, it is interesting to see a sudden abrupt change due to SPs or the RWA. In order to confirm its physical origin, one can use equations (1) and (2). For example, to obtain good focusing or a high intensity in the grating structure, $k$ in equation (1) should be large, which corresponds to $\tan(k_g h) \to 0$, i.e., the grating grooves act as quarter-wavelength antennas ($k_g = k_0$) [45]. Thus, the SP resonance occurs when $h \approx \lambda/4 = 150$ nm, which is not equal to the calculated grating thickness. In contrast, the RWA might occur at peak D due to one diffraction order emerging at the grating angle. For example, from equation (2) $\Lambda$ is equal to $\lambda$ when $\theta = 0°$ and $j = 1$ and its value agrees well with the computed grating period ($\Lambda = 600$ nm).

Figure 6(c) plots the emittance at peak H with its value being greater than 0.8 from $\theta = 0°$ to 70°, and it then decreases to zero when $\theta$ reaches 90°, while that at peak G exhibits a value greater than 0.75 from $\theta = 0°$ to 70° and then also drops to zero. Figure 6(d) shows that the emittance fluctuates greatly when the angle of incidence changes; for example, at peaks K and L it drops fast to 0.8 and 0.5 from $\theta = 0°$ to 60° and to 40°, respectively. In figures 6(c) and (d), the small peaks disappear or emerge at shorter wavelengths as

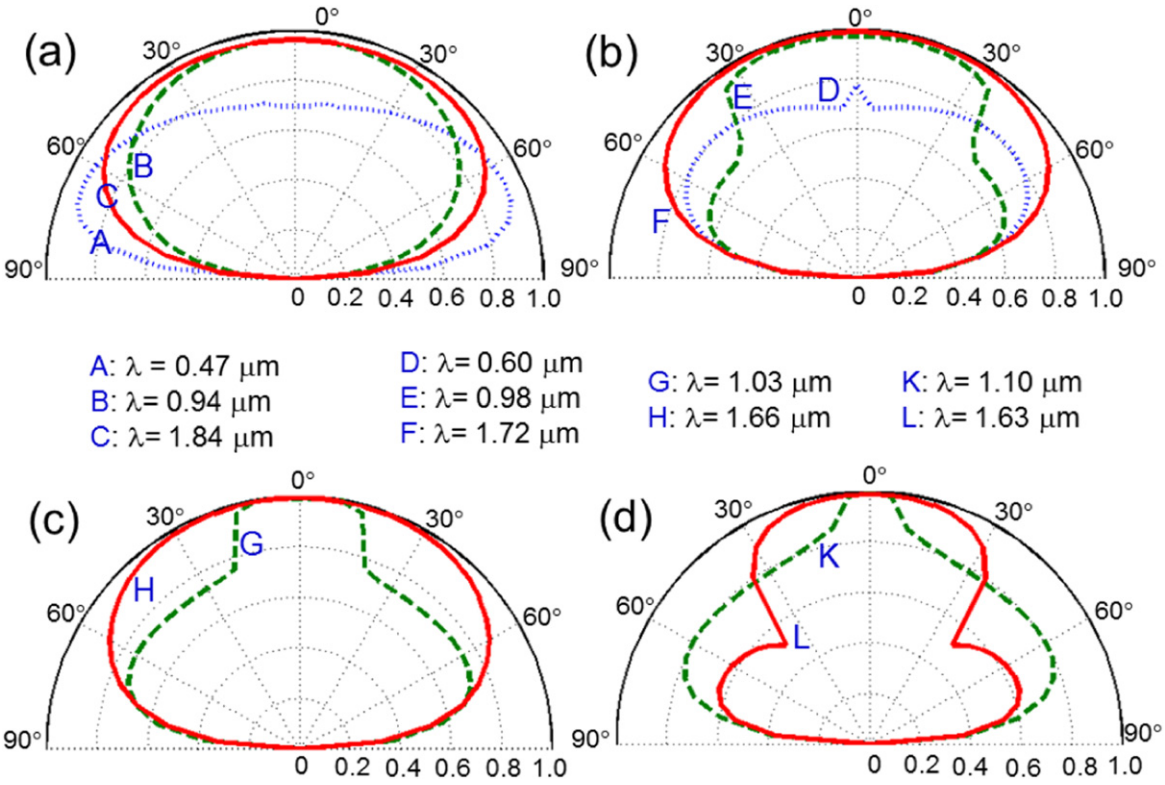


**Figure 6.** Polar plot of emittance spectra for TM waves at peaks A, B, C, E, F, G, H, K, and L.

compared with those shown in figures 4(a) and (b). Moreover, the emittance peaks show the highest value at a wide wavelength range of 0.6 ∼ 1.72 $\mu$m. Overall, the results presented in figure 6 illustrate that the grating structures with $\Lambda = 600$ and 800 nm provide very high emittance for TPV emitters. Further, the excitation (peak D) has been demonstrated analytically and is known by the RWA, while that at the largest peak is verified using TM field and Poynting vector distributions, as illustrated in figure 7.

Figure 7 shows magnetic field and the time-average Poynting vector patterns at peaks D1, D2, and D at the same wavelength ($\lambda = 0.6\,\mu$m), E ($\lambda = 0.98\,\mu$m), F ($\lambda = 1.72\,\mu$m), G ($\lambda = 1.03\,\mu$m), H ($\lambda = 1.66\,\mu$m), and I and J at the same wavelength ($\lambda = 0.8\,\mu$m) within two grating periods shown in figures 4(b) and (c). The background of the figures is the *y*-component intensity of magnetic fields while vectors indicate the time-average Poynting energy density. It is seen that magnetic field and Poynting distributions at peak $D_1$ are different from those at $D_2$ and D. Based on these plots and equations (1) and (2), one may conclude that the SPs occur at peak $D_1$ due to the energy, indicated by Poynting vectors, oscillating at the W horizontal boundaries (see figure 7 for peak $D_1$) while the RWA is excited at peaks $D_2$ and D ($\Lambda$ equal to $\lambda$ confirmed by equation (2)). However, magnetic field and Poynting vector patterns of peaks E, F, G, and H are similar. It is observed that the TM waves are standing in the groove grating regions which causes an enhancement of the emittance. In addition, from equation (3) the maximum resonance $\lambda_{lmn}$ can be obtained by setting $l = n = 0$, and it results in $\lambda_{lmn} = 4h_{\text{total}}$. As can be seen, magnetic fields at peaks E, F, G, and H concentrate mostly in the grating grooves with a thickness of 400 nm, and these peaks exist at $\lambda_{\max} \approx 1.6\,\mu$m. Similarly, peaks I and J are excited by the SPs ($h \approx \lambda/4 = 200$ nm) and the RWA ($\Lambda = \lambda = 800$ nm,) respectively, as clearly demonstrated by Poynting vector patterns shown in figure 7 and equations (1) and (2). However, it is interesting that the merging of these peaks results in an increase of the emittance at $\lambda = 800$ nm, as shown in figure 4(c).

Overall, the results presented in figure 7 with the analytical solutions demonstrated in equations (1)–(3) confirmed that the enhancement of magnetic fields in the grating structure with $\Lambda = 800$ nm at the short wavelength is due to the interplay of the SPs and the RWA, while the maximum emittance at longer wavelengths obtained from both optimized gratings is attributed to the CR modes.

## 5. Emitter-based pyramid grating structure made of nickel

In order to demonstrate the design feasibility, we introduce another emitter made of nickel, a material withstanding high temperatures suitable for TPV applications. Figure 8(a) shows the emittance spectrum of a hybrid Ni grating structure with the same geometric parameters as those in figure 4. It is found that the grating has a similar spectral feature to that of the W grating structure. The Ni grating structure emits an average

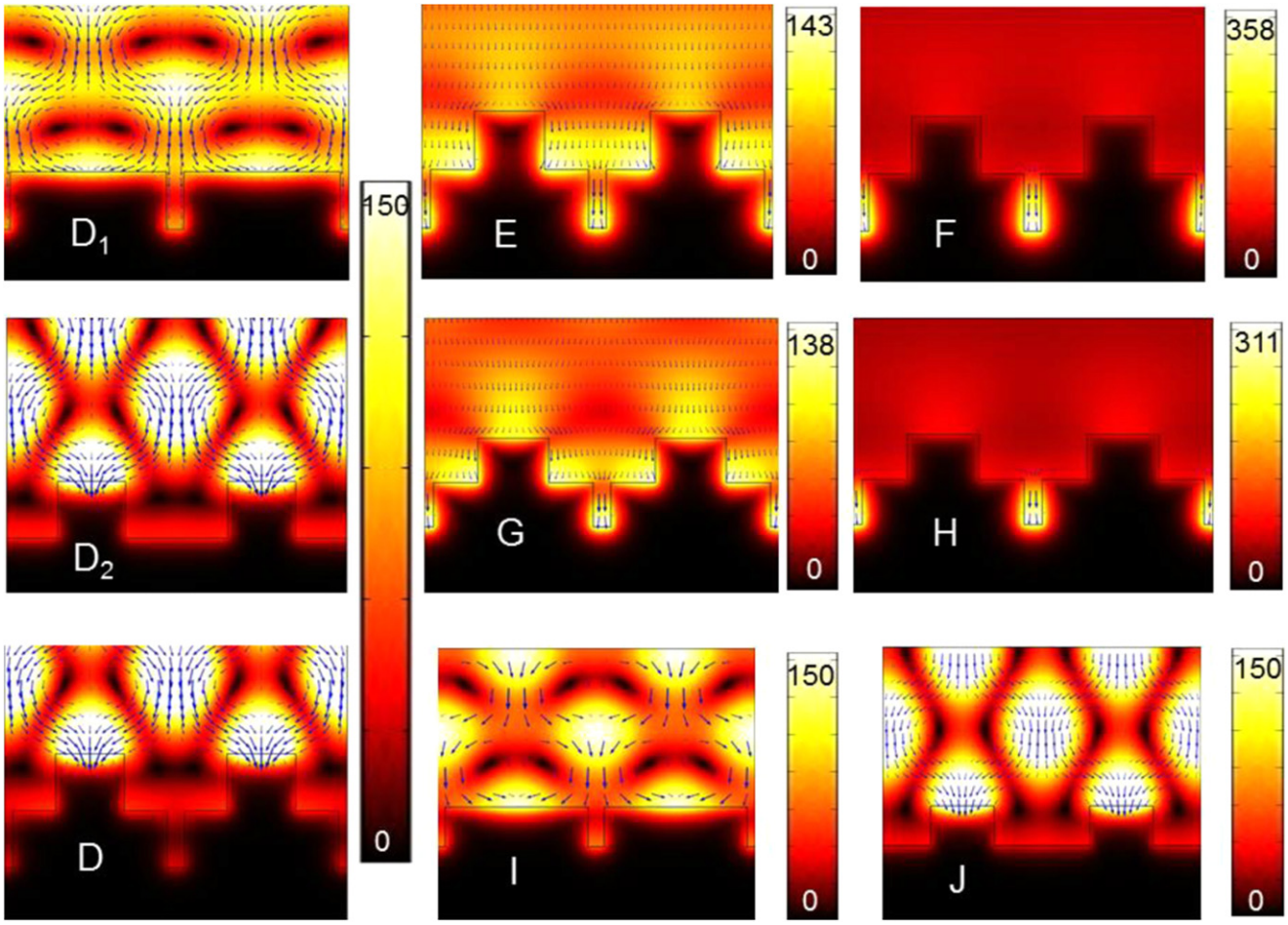


**Figure 7.** Near-field patterns of grating structures for normal TM wave incidence at peaks $D_1$, $D_{2,}$ and D at same $\lambda = 0.6\ \mu$m, E ($\lambda = 0.98\ \mu$m), F ($\lambda = 1.72\ \mu$m), G ($\lambda = 1.03\ \mu$m), H ($\lambda = 1.66\ \mu$m), and I and J at the same $\lambda = 0.8\ \mu$m. Note that the figures represent magnetic field distributions in the background and time-average Poynting vectors.

intensity less than the W grating does. However, the grating structures with $\Lambda = 600$ nm (the dashed line) nm and 800 nm (the dotted line) display high emittance in the wavelength range of interest. Figures 8(b) and (c) show contour plots of the emittance of these structures as a function of the wavelength and the angle of incidence. It is observed that the combined Ni grating with $\Lambda = 600$ nm emits higher energy in the wavelength range of interest at angles from $\theta = 0°$ to $\theta = 70°$ than the one with $\Lambda = 800$ nm. Generally speaking, the pyramid Ni grating also provides high optical performance for TPV applications. Although grating made of Ni is relatively cost-effective and easier to machine, it absorbs energy less than the W grating structure as demonstrated in figures 4(b) and (c).

## 6. Conclusions

We have proposed a pyramid grating structure made of W and Ni that has nearly perfect emittance by combining two single-layered gratings with a low and high metal filling ratio in a grating region. The results have shown that the enhanced emittance at the wavelengths of interest from 0.6 $\mu$m to 1.72 $\mu$m is due to the interplay between the SPs and the RWA at short wavelengths, and the CR modes at longer wavelengths. The physical origin was also validated by analytical demonstrations of the excited modes. Moreover, it has been shown that the broad spectrum is insensitive to the angle of incidence from 0° to 70°. This study may pave the way for designs of the plasmonic nanostructures for energy harvesting applications based on extraordinary optical absorption enhancement.

## Acknowledgments

The authors gratefully acknowledge the support by IT4Innovations with the project CZ. 1.05/1.1.00/02.0070, Post-Doci project Opportunity for young researchers No. #CZ.1.07/2.3.00/30.0016, and the Grand Agency of Czech Republic (#15-21547S); and by Natural Sciences and Engineering Research Council (NSERC), Collaborative Research and Training Experience, and Applied Science in Photonics and Innovative Research in Engineering (ASPIRE) programs of Canada. NN-H is very thankful to Professors Y-L Lo and Y-B Chen (NCKU) for discussions on the RCWA.

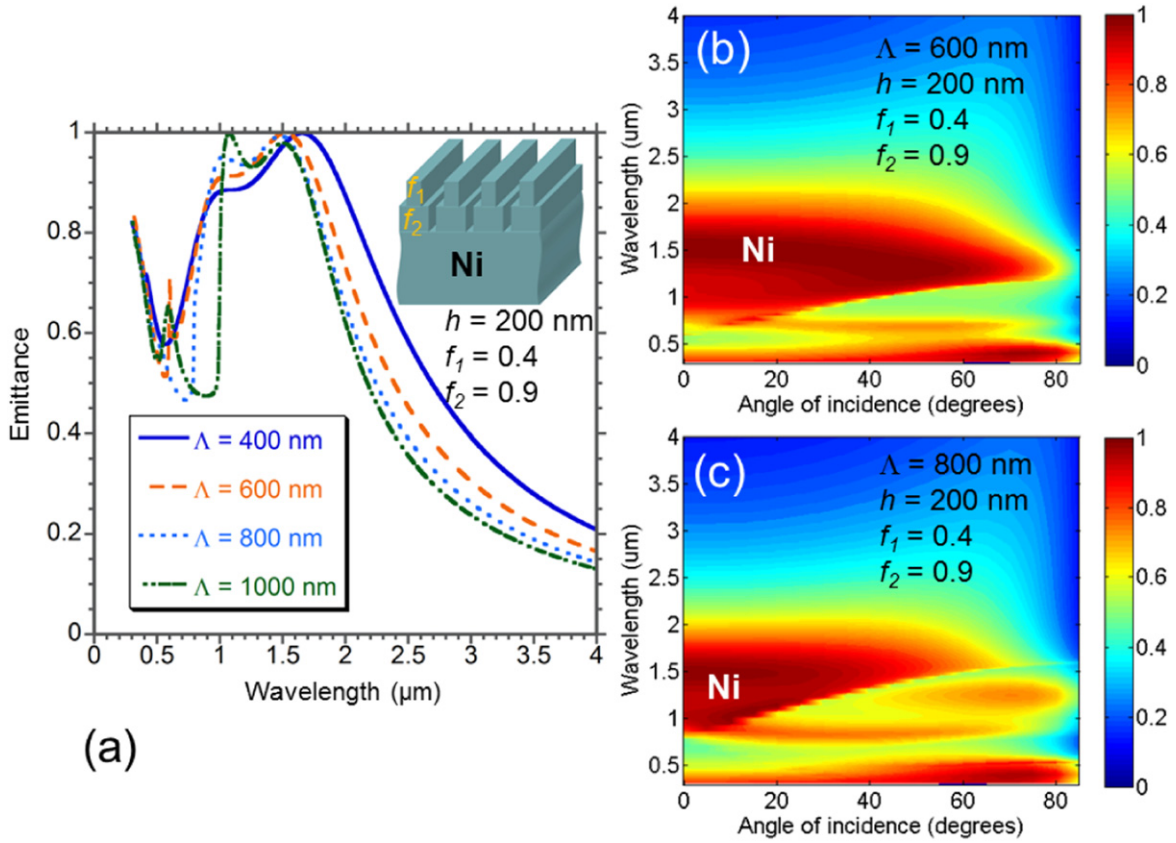


**Figure 8.** (a) Emittance spectrum of a hybrid grating structure made of nickel with different grating periods; (b) and (c) contour plots of the Ni grating with $\Lambda = 600$ nm and $\Lambda = 800$ nm as function of wavelength and angle of incidence.

## References


[1] Basu S, Chen Y B and Zhang Z 2007 Microscale radiation in thermophotovoltaic devices—a review *Int. J. Energy Res.* **31** 689–716

[2] Narayanaswamy A and Chen G 2004 Thermal emission control with one-dimensional metallodielectric photonic crystals *Phys. Rev.* B **70** 125101

[3] Wu C, Burton Neuner I, Shvets G, John J, Milder A, Zollars B and Savoy S 2011 Large-area wide-angle spectrally selective plasmonic absorber *Phys. Rev.* B **84** 075102

[4] Ye Y-H, Jiang Y-W, Tsai M-W, Chang Y-T, Chen C-Y, Tzuang D-C, Wu Y-T and Lee S-C 2008 Localized surface plasmon polaritons in $Ag/SiO_2/Ag$ plasmonic thermal emitter *Appl. Phys. Lett.* **93** 033113

[5] Diem M, Koschny T and Soukoulis C M 2009 Wide-angle perfect absorber/thermal emitter in the terahertz regime *Phys. Rev.* B **79** 033101

[6] Nguyen-Huu N, Cada M and Pistora J 2014 Investigation of optical absorptance of one-dimensionally periodic silicon gratings as solar absorbers for solar cells *Opt. Express* **22** A68–79

[7] Hesketh P J, Zemel J N and Gebhart B 1986 Organ pipe radiant modes of periodic micromachined silicon surfaces *Nature* **324** 549–51

[8] Wang L and Zhang Z 2012 Wavelength-selective and diffuse emitter enhanced by magnetic polaritons for thermophotovoltaics *Appl. Phys. Lett.* **100** 063902

[9] Nguyen-Huu N, Chen Y-B and Lo Y-L 2012 Development of a polarization-insensitive thermophotovoltaic emitter with a binary grating *Opt. Express* **20** 5882–90

[10] Ungaro C, Gray S K and Gupta M C 2014 Graded-index structures for high-efficiency solar thermophotovoltaic emitting surfaces *Opt. Lett.* **39** 5259–62

[11] Chen Y-B and Zhang Z M 2007 Design of tungsten complex gratings for thermophotovoltaic radiators *Opt. Commun.* **269** 411–7

[12] Maruyama S, Kashiwa T, Yugami H and Esashi M 2001 Thermal radiation from two-dimensionally confined modes in microcavities *Appl. Phys. Lett.* **79** 1393–5

[13] Greffet J-J, Carminati R, Joulain K, Mulet J-P, Mainguy S and Chen Y 2002 Coherent emission of light by thermal sources *Nature* **416** 61–4

[14] Kreiter M, Oster J, Sambles R, Herminghaus S, Mittler-Neher S and Knoll W 1999 Thermally induced emission of light from a metallic diffraction grating, mediated by surface plasmons *Opt. Commun.* **168** 117–22

[15] Chen Y-B and Tan K-H 2010 The profile optimization of periodic nano-structures for wavelength-selective thermophotovoltaic emitters *Int. J. Heat Mass Transfer* **53** 5542–51

[16] Zhao B, Wang L, Shuai Y and Zhang Z M 2013 Thermophotovoltaic emitters based on a two-dimensional grating/thin-film nanostructure *Int. J. Heat Mass Transfer* **67** 637–45

[17] Lee J H, Kim Y S, Constant K and Ho K M 2007 Woodpile metallic photonic crystals fabricated by using soft lithography for tailored thermal emission *Adv. Mater.* **19** 791–4

[18] Hao J, Wang J, Liu X, Padilla W J, Zhou L and Qiu M 2010 High performance optical absorber based on a plasmonic metamaterial *Appl. Phys. Lett.* **96** 251104

[19] Butun S and Aydin K 2014 Structurally tunable resonant absorption bands in ultrathin broadband plasmonic absorbers *Opt. Express* **22** 19457–68

[20] Wu C, Neuner B III, John J, Milder A, Zollars B, Savoy S and Shvets G 2012 Metamaterial-based integrated plasmonic absorber/emitter for solar thermo-photovoltaic systems *J. Opt.* **14** 024005
[21] Nam Y, Yeng Y X, Lenert A, Bermel P, Celanovic I, Soljačić M and Wang E N 2014 Solar thermophotovoltaic energy conversion systems with two-dimensional tantalum photonic crystal absorbers and emitters *Sol. Energy Mater. Sol. Cells* **122** 287–96
[22] Garín M, Hernández D, Trifonov T and Alcubilla R 2015 Three-dimensional metallo-dielectric selective thermal emitters with high-temperature stability for thermophotovoltaic applications *Sol. Energy Mater. Sol. Cells* **134** 22–8
[23] Yeng Y X, Ghebrebrhan M, Bermel P, Chan W R, Joannopoulos J D, Soljačić M and Celanovic I 2012 Enabling high-temperature nanophotonics for energy applications *Proc. Natl Acad. Sci.* **109** 2280–5
[24] Sai H, Kanamori Y and Yugami H 2003 High-temperature resistive surface grating for spectral control of thermal radiation *Appl. Phys. Lett.* **82** 1685–7
[25] Heine C and Morf R H 1995 Submicrometer gratings for solar energy applications *Appl. Opt.* **34** 2476–82
[26] Lee B J, Chen Y-B, Han S, Chiu F-C and Lee H J 2014 Wavelength-selective solar thermal absorber with two-dimensional nickel gratings *J. Heat Transfer* **136** 072702
[27] Wang X, Flicker J, Lee B, Ready W and Zhang Z 2009 Visible and near-infrared radiative properties of vertically aligned multi-walled carbon nanotubes *Nanotechnology* **20** 215704
[28] Sai H, Kanamori Y, Hane K and Yugami H 2005 Numerical study on spectral properties of tungsten one-dimensional surface-relief gratings for spectrally selective devices *J. Opt. Soc. Am.* A **22** 1805–13
[29] Sergeant N P, Agrawal M and Peumans P 2010 High performance solar-selective absorbers using coated sub-wavelength gratings *Opt. Express* **18** 5525–40
[30] Lin S Y, Moreno J and Fleming J G 2003 Three-dimensional photonic-crystal emitter for thermal photovoltaic power generation *Appl. Phys. Lett.* **83** 380–2
[31] Han S E, Stein A and Norris D J 2007 Tailoring self-assembled metallic photonic crystals for modified thermal emission *Phys. Rev. Lett.* **99** 053906
[32] Nagpal P, Han S E, Stein A and Norris D J 2008 Efficient low-temperature thermophotovoltaic emitters from metallic photonic crystals *Nano Lett.* **8** 3238–43
[33] Nguyen-Huu N and Lo Y-L 2013 Tailoring the optical transmission spectra of double-layered compound metallic gratings *IEEE Photonics J.* **5** 2700108
[34] Nguyen-Huu N and Lo Y-L 2013 Control of infrared spectral absorptance with one-dimensional subwavelength gratings *J. Lightw. Technol.* **31** 2482–90
[35] Cui Y, Fung K H, Xu J, Ma H, Jin Y, He S and Fang N X 2012 Ultrabroadband light absorption by a sawtooth anisotropic metamaterial slab *Nano Lett.* **12** 1443–7
[36] Boltasseva A and Shalaev V M 2008 Fabrication of optical negative-index metamaterials: recent advances and outlook *Metamaterials* **2** 1–17
[37] Rakic A D, Djurisic A B, Elazar J M and Majewski M L 1998 Optical properties of metallic films for vertical-cavity optoelectronic devices *Appl. Opt.* **37** 5271–83
[38] Zhang Z M 2007 *Nano/Microscale Heat Transfer* (New York: McGraw-Hill)
[39] Nguyen-Huu N, Cada M and Pistora J 2014 Imperfectly geometric shapes of nanograting structures as solar absorbers with superior performance for solar cells *Opt. Express* **22** A282–94
[40] Tseng A A, Chen K, Chen C D and Ma K J 2003 Electron beam lithography in nanoscale fabrication: recent development *IEEE Trans. Electron. Packag. Manuf.* **26** 141–9
[41] Shinji M and Yukinori O 1996 Focused ion beam applications to solid state devices *Nanotechnology* **7** 247
[42] Guo L J 2007 Nanoimprint lithography: methods and material requirements *Adv. Mater.* **19** 495–513
[43] Beermann J, Eriksen R L, Søndergaard T, Holmgaard T, Pedersen K and Bozhevolnyi S I 2013 Plasmonic black metals by broadband light absorption in ultra-sharp convex grooves *New J. Phys.* **15** 073007
[44] Bett A and Sulima O 2003 GaSb photovoltaic cells for applications in TPV generators *Semicond. Sci. Technol.* **18** S184
[45] Rusina A, Durach M and Stockman M I 2010 Theory of spoof plasmons in real metals *Proc. SPIE* **7757** 77572R
[46] Wood R 1902 XLII On a remarkable case of uneven distribution of light in a diffraction grating spectrum *Phil. Mag.* **4** 396–402